ISSN No:-2456-2165 https://doi.org/10.38124/ijisrt/IJISRT24JUL1249

Influence of Process Parameters on Residual Stresses in Dissimilar Friction Stir Welding of Aluminum Alloys

Zulqarnain Sarfaraz[1]; Dr. Hasan Aftab Saeed[2]
Department of Mechanical Engineering, CEME
National University of Sciences and Technology Islamabad, Pakistan

Correspondence Email: zsarfaraz.me19ceme@me.ceme.edu.pk

Abstract:- Foreseeing how welded structures will behave requires careful consideration of the residual stresses that the friction stir welding (FSW) process introduces. These residual stresses can cause severe deformation and compromise the ability of friction stir welded structures to bear imposed external loads. This work uses a Sequentially Coupled Thermo-mechanical finite element simulation to quantitatively evaluate the influence of such residual stresses coming from the FSW process. This modelling method examines the thermal and post-weld stress distributions during the friction stir welding of dissimilar AA2024-T3 and AA5086-O alloys. The procedure entails an initial thermal analysis followed by a mechanical analysis to determine the distribution of residual stresses across the entire dissimilarly welded alloys. The study examined how alterations in FSW operational parameters, such as rotational and translational speeds, influence both the thermal conditions and residual stress distribution. The findings highlighted that both temperature and residual stress exhibited higher values on the retreating side of the specimen compared to the intended advancing side. As the tool rotational speed rose, the magnitude of longitudinal residual stress dropped, however it showed an increase with greater tool translational speeds. Moreover, the simulated outcomes demonstrate the substantial impact of welding fixtures on the profiles and magnitudes of residual stresses.

Keywords:- *Friction Stir Welding, Thermomechanical Model, Dissimilar Joints of Aluminum Alloys, Residual Stresses.*

I. INTRODUCTION

Friction Stir Welding (FSW) is a contemporary metal joining technique pioneered by Wayne Thomas and his team at the Welding Institute (TWI) in 1991 [1]. Unlike traditional welding techniques, FSW is categorized as a solid-state joining method due to the material being welded is not melted throughout the process [1]. This feature makes FSW particularly suitable for applications in industrial sectors like marine, automotive, and aircraft, where the characteristics of the metal to remain as intact as feasible after welding. In aerospace applications, AA2024-T3 and AA5086-O are both frequently used materials. FSW of these dissimilar aluminum alloys are used to attach intricate structural parts including fuselage sections, wings, and aircraft panels. FSW provides prospective uses for building lightweight, fuel-efficient automobiles in the automotive industry. The joint characteristics of AA2024-T3 and AA5086-O alloys can benefit components like chassis parts, frames, and panels. The usage of FSW for combining the AA2024-T3 and AA5086-O is crucial for the shipbuilding sector [2]. Technologies for renewable energy use aluminum alloys. FSW joints of AA2024-T3 and AA5086-O can be utilized in the production of solar panels, wind turbine parts, and other renewable energy infrastructure.

Due to its potential to produce strong, lightweight structures for the aerospace, automotive, and marine sectors, dissimilar friction stir welding (FSW) of the aluminum alloys AA2024-T3 and AA5086-O has attracted a lot of attention. Residual stresses, which have the potential to undermine structural integrity, continue to pose a serious problem. During FSW, complex interactions between mechanical and thermal elements lead to residual stresses, with process parameters playing a crucial role. Numerous researchers have developed mathematical and experimental techniques to forecast welding residual stresses. The ability to analyze residual stresses in welded components has become much more advanced because of developments in computer technology and methodologies like the finite element approach.

To investigate how heat was transferred into the plate, Gould et al. created an analytical model based on the Rosenthal equation that solely evaluate heat produced [3]. In this study, a line contact in the shape of a ring was postulated between the shoulder and workpiece in command to find out the impact of frictional heat. The variation in temperature was discovered to be asymmetrical, with the leading edge being much cooler than the trailing edge. This resulted from the fact that the tool's leading edge heated cold material while the trailing edge heated metal that had been heated by the tool's leading edge. Armansyah utilized the FE procedure to examine the temp distribution in FSW [4]. Thermal FE studies are carried out for this aim to simulate the temperature profile and its characteristics in weld regions with regard to welding method’s factors like rotating and travel speed. The findings demonstrate that increasing tool rotating speed while preserving a fixed transverse speed

ISSN No:-2456-2165 https://doi.org/10.38124/ijisrt/IJISRT24JUL1249

would result in an upsurge in the quantity of heat produced in weld regions. Whereas, raising the translational speed will result in less heat being produced in weld zones while maintaining consistent tool pin-shoulder rotational rates. Abdul Arif used K-type thermocouples, temperature fluctuations in various places were monitored during welding tests [5]. Due to its smoother composition and better thermal conductivity, which allows for the distribution of the majority of the heat created at the contact to AA6061, only AA6061 will be used in both circumstances as flash. Due to AA5086's greater hardness value, lower heat conductivity, and higher melting point, displacement is hardly noticeable. The weld interface's temperature is insufficient to sufficiently plasticize AA5086. Due to a greater quantity of heat being transported to Al-6061, the heat affected zone of AA6061 exceeds than AA5086.

Weld zone stress was noted by Peel et al. to exist in both longitudinal and transverse directions. According to experimental findings, longitudinal stress grew with traverse speed [6]. This rise was most likely brought on by welding with greater heat gradients and less time for stress release. Chen and Kovecevic investigated the connection between tool traverse speed and the predicted residual stresses [7]. The shoulder's mechanical impact was taken into account in the mechanical model because it was anticipated that the shoulder's fairly broad contact zone with the workpiece would be responsible for a significant amount of the mechanical stress. It was predicted that the weld's stress distribution would change after the welded plates were removed from the clamp. Zhang et al. created a 2D finite element model based on solid mechanics to investigate flowing trends and residual stresses [8]. The maximum longitudinal residual stress might grow as the translational velocity increased. Additionally, because of the fixture's mechanical restraints on the plates, the tool's rotational and transverse motions would add to the tension in the weld. To acquire residual stress distributions, the temperature of the plate would be lowered to 25ºC, followed by the removal of the clamp. H. Jamshidi Aval investigated thermal profiles and residual stresses in different FSW of AA5086 and AA6061 alloys using both empirical and analytical method [9]. The study found that the tool traverse rate predominantly influences the spread of transverse residual stresses, but the tool's rotation rate has a significant impact on the amount of the peak tensile residual stress. A spike in thermal input for each portion of the welded joint causes higher residual tensile stresses and a bigger impacted region. Furthermore, it was discovered that the mechanical constraint imposed by the welding clamps have a significant impact on the residual stress pattern, with the highest residual stress decreasing as the clamps are promptly released. Thermo-mechanical modeling for residual stresses of FSW of dissimilar alloys was explored by Abdul Arif [10]. After 15 seconds, AA5086-O on the leading side and AA6061-T6 on the trailing side are used to measure lateral and perpendicular residual stresses. According to the estimations, the highest lateral stress is greater than the maximum transverse stress, and the peak longitudinal compressive stress spreads across the rotating pin, whereas the greatest longitudinal tensile stress is primarily generated near the specimen's edge. Using X-ray Diffraction, J. Zapataa [11] studied the impact of rotational and translational rates on the residual stresses of AA2024-T3 and AA6061-T6. The change in rotational speed was associated with the biggest differences in the behavior and size of residual stresses. The amplitude of the longitudinal residual stresses is reduced when the rotating speed is increased. This was strongly related to the rise in temperature intake and the fall in thermal misfit across the various weld zones.

The study of A. Brahami employed numerical simulation techniques to model and analyze the thermal and mechanical responses during the FSW process of AA6061-T6 [12]. The findings highlighted that specific welding parameters significantly affect the peak temperature and stress distribution, providing insights for optimizing FSW processes to enhance joint quality and reduce residual stresses. In a study conducted by Kareem N. Salloomi [13], the investigation delved into estimating thermal and residual stress conditions in dissimilar FSW of aluminum alloys. Specifically, the alloys studied were AA6061-T6 and AA2024-T3. To assess these conditions, a Coupled Eulerian-Lagrangian (CEL) finite element analysis was employed during the FSW process. The research revealed that the most significant factor influencing the results was the longitudinal residual stress, which was greater in the AA6061 portion compared to the AA2024 portion. Interestingly, this fraction of residual stress reduced with a raise in the tool's rotational speed. However, it increased when the tool's traversal speed was raised as well. In contrast to the longitudinal factor, the transverse phase displayed minimal amounts of residual stress. The findings for the residual stresses support the notion that rotating speed of the tool has a greater impact than its traversal speed. Ivan S. Zuiko investigated the dissimilar friction stir welding of AA2519 and AA5182 aluminum alloys [14]. Friction stir welding experiments were conducted, and the resulting welds were analyzed using mechanical testing and microstructural examinations. The study found that the optimal welding parameters improved joint efficiency, mechanical properties, and microstructural characteristics of the dissimilar aluminum alloy welds.

Dissimilar friction stir welding (FSW) joints have been the subject of a lot of experimental study; nevertheless, there aren't many studies that concentrate on modelling residual stress assessment. In order to address this gap, a 3D Sequentially Coupled Thermo-mechanical finite element simulation is used in this work to forecast residual stress in the FSW of the AA2024-T3 and AA5086-O joints and to analyze the thermal environment. In contrast to earlier research, this model takes into account the impact of changing traverse and rotational speeds on residual stresses in addition to a nonlinear friction coefficient and convective thermal boundary conditions. The outcome of the model is linked with the issued results of Kareem N. Salloomi [13] for the validation of the generated model. This thermomechanical model is then utilized to evaluate the process for AA5086-O and AA2024-T3. For the investigation of the impacts of different proceeding variables on thermal profiles and residual stress

ISSN No:-2456-2165 https://doi.org/10.38124/ijisrt/IJISRT24JUL1249

in the work-piece, the model is then extended to perform parametric investigations.

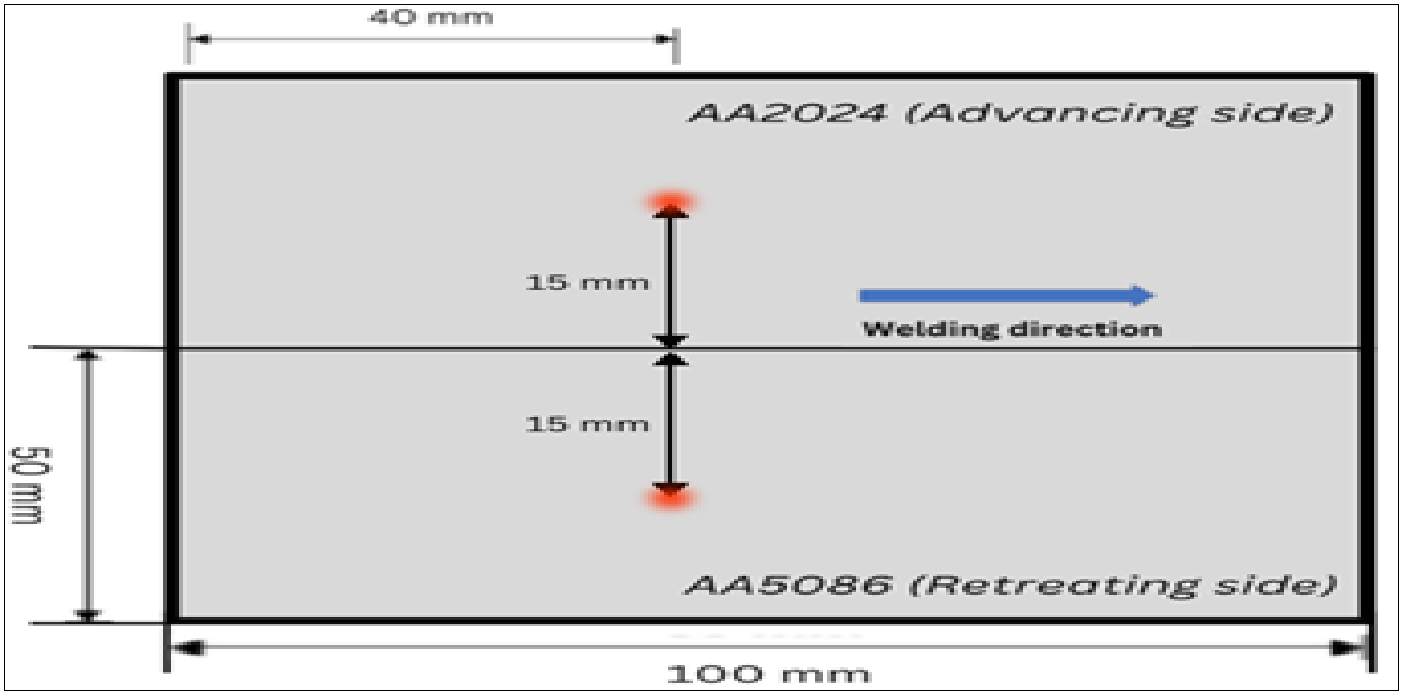

Fig 1: Schematic Diagram of the Workpiece Used in FSW Showing Temperature Locations

II. SEQUENTIALLY COUPLED THERMOMECHANICAL MODEL

By breaking down complicated continuum problems into a number of smaller, related issues, the Finite Element Method (FEM) provides a process for solving intricate persistent issues. The most frequent application of FEM is in numerical analysis, where it is utilized to produce approximations of solutions to an extensive range of engineering issues [15]. The numerical simulation of the FSW method in the current work is conducted using the commercial general-purpose FE programme ABAQUS/Standard. In this context, finite element models are harnessed to explore the thermal and mechanical responses of materials as they undergo the dissimilar FSW method involving AA5086-O and AA2024-T3 alloys. The AA5086-O alloy is selected to be on the re-treating side for all the welded specimens whereas the AA2024-T3 alloy is opted to be on the advancing side. A sequentially coupled thermomechanical model is created for investigation in this work. To calculate the temperature fields, heat transfer model is first created. Following this, projections for distortions and residual stresses are made by utilizing the temperature fields as inputs into a three-dimensional structural model that incorporates nonlinearity and rate dependence. Subsequently, the study delves into exploring the influence of various proceeding variables, such as rotational and transverse speed. To validate the accuracy of the models, the results are then compared to established numerical data.

III. THERMAL MODELLING

The Fourier law presupposes the energy equation that governs heat conduction [16]. The equation that regulates for temperatures becomes the 3-D transient and the originating factor from the entire procedure.

$$k\left(\frac{\partial^2 T}{\partial x^2}+\frac{\partial^2 T}{\partial y^2}+\frac{\partial^2 T}{\partial z^2}\right)+Q_{\text{int}}=c\rho\frac{\partial T}{\partial t} \quad (1)$$

By using the Galerkin's weighted residual approach the finite element equation (1) and its corresponding boundary conditions can be expressed in matrix form:

$$T^e(x,y,z,t)=\{N(x,y,z)\}^{eT}\{T\}^e$$
$$\frac{\partial T^e}{\partial t}=\{N(x,y,z)\}^{eT}\{\dot{T}\}^e \quad (2)$$

Where,

$$\{\dot{T}\}^e=\begin{Bmatrix}\frac{\partial T_1}{\partial t}\\ \frac{\partial T_2}{\partial t}\\ \vdots\\ \frac{\partial T_i}{\partial t}\end{Bmatrix}$$

$$[C]^e\{\dot{T}\}^e+([K_c]^e+[K_h]^e+[K_r]^e)\{T\}^e=\{R_Q\}^e+\{R_q\}^e+\{R_h\}^e+\{R_r\}^e \quad (3)$$

ISSN No:-2456-2165 https://doi.org/10.38124/ijisrt/IJISRT24JUL1249

Here,

Capacitive matrix $$[C]^e = \int_V \rho c_p \{N\}^e \{N\}^{eT} dV \quad (4)$$

Convective matrix $$[K_h]^e = \int_{S_h} h\{N\}^s \{N\}^{sT} dS \quad (5)$$

Conductive matrix $$[K_c]^e = \int_V [B]^e [D]^e [B]^{eT} dV \quad (6)$$

Radiative matrix $$[K_r]^e = \int_{S_r} \sigma \varepsilon T^4 \{N\}^s dS \quad (7)$$

And

$$\{R_Q\}^e = \int_V Q_{\text{in}} \{N\}^e dV$$

$$\{R_q\}^e = \int_{S_q} \{N\}^s \{q_s\}^s dS$$

$$\{R_h\}^e = \int_{S_h} hT_\infty \infty \{N\}^s dS$$

$$\{R_r\}^e = \int_{S_r} \alpha q_r \{N\}^s dS$$

Where,

$$\{N\}^e = \begin{Bmatrix} N_1 \\ N_2 \\ \vdots \\ N_i \end{Bmatrix}^e$$

$$[D]^e = \begin{bmatrix} k_x & 0 & 0 \\ 0 & k_y & 0 \\ 0 & 0 & k_z \end{bmatrix}, \quad [B]^{eT} = \begin{bmatrix} \frac{\partial N_1}{\partial x} & \frac{\partial N_2}{\partial x} & \frac{\partial N_3}{\partial x} & \cdots & \frac{\partial N_i}{\partial x} \\ \frac{\partial N_1}{\partial y} & \frac{\partial N_2}{\partial y} & \frac{\partial N_3}{\partial y} & \cdots & \frac{\partial N_i}{\partial y} \\ \frac{\partial N_1}{\partial z} & \frac{\partial N_2}{\partial z} & \frac{\partial N_3}{\partial z} & \cdots & \frac{\partial N_i}{\partial z} \end{bmatrix}^e$$

The FE thermal model is constructed under some presumptions i.e., work-piece composition is homogenous and isotropic, the welding procedure doesn't involve any melting and the weld centerline is subject to identical thermal boundary conditions. The two plates have dimensions of 5 mm thickness, 100 mm length, and 50 mm width. The AA5086-O alloy was selected to be on the re-treating side of all the welded specimens whereas the AA2024-T3 alloy was opted to be on the advancing side. The tool's dimensions are 20 mm in diameter for the concave shoulder, 4 mm in diameter for the threaded pin, and 4.7 mm is the pin height. The downward force (axial force) on the tool is 7 KN.

The dissimilar Aluminum sheets were meshed using DC3D8R elements in three dimensions. There are 18894 individual elements in the mesh. These elements are linear hexahedral elements of type DC3D8R. There are 25840 nodes in the mesh as a whole.

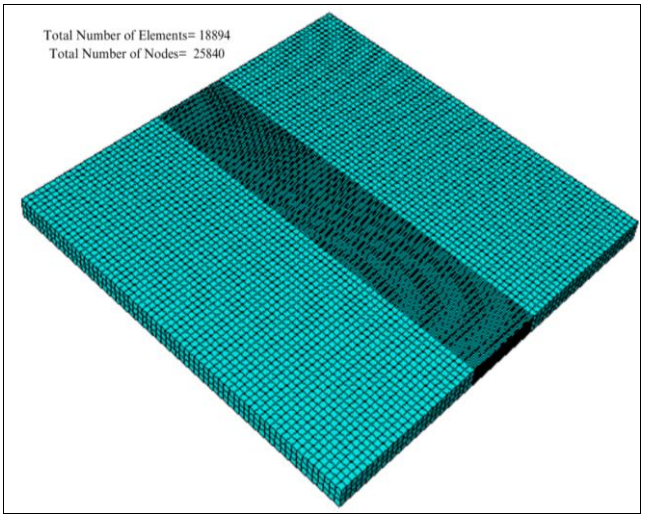

Fig 2: Mesh Development using DC3D8R Elements

Table 1: Thermal and Structural Properties Of Aa 2024-T3 [13]

Material	Temperature (°C)	Thermal Conductivity (W/m°C)	Specific heat (J/kg°C)	Thermal Expansion (10^{-6}/°C)	Young's Modulus (Gpa)	Density (kg/m^3)
AA 2024-T3	25	121	875	22	72	2770
	37.8	124	895	23	71.9	
	93.3	128	906	23.5	66.5	
	148.9	139	925	24.5	63.5	
	204.4	153	950	24.8	63	
	260	172	990	25.3	57.1	
	315.6	178	1040	25.5	51.4	
	371.1	182	1080	26	47.3	
	426.7	190	1110	26.6	44	

ISSN No:-2456-2165 https://doi.org/10.38124/ijisrt/IJISRT24JUL1249

Table 2: Thermal and Structural Properties of Aa 5086-O [9]

Material	Density (Kg/m³)	Thermal expansion (α)		Thermal conductivity (k)		Specific heat capacity (c_p)		Young's modulus (E)	
		$10^{-6}/°C$	Temp(°C)	W/m°C	Temp (°C)	J/kg°C	Temp (°C)	GPa	Temp (°C)
AA 5086-O	2657	23.8	25	127	25	900	25	70.0	25
		25.5	200	151	250	960	250	67.8	100
		26.8	300	154	300	980	300	60.7	200
		28.9	400	158	400	1020	400	51.0	300
		31.5	500	169	500	1113	500	37.4	400

Surface loads were given as the boundary conditions for the FSW thermal model using ABAQUS codes. Data gathered from published research publication [13] was used to form implications for various boundary conditions. All of the workpiece's free surfaces lose heat to the environment convectively and radiatively, while conduction damages happen from the beneath surface to the supporting plate. The heat loss q_h is estimated using equation (9), taking into account convection and radiation across each workpiece regions aside from the bottom. On all work-piece surfaces, excluding the bottom, an adequate convection and radiation were estimated accordingly. The heat loss rate q_h is indicated by:

$$q_h = h_{con}(T - T_0) + \varepsilon\sigma(T^4 - T_0^4) \quad (8)$$

Where, T is the work-piece's absolute temperature, T_0 is the sink temperature, h_{con} is the convective film coefficient, ε is the emissivity constant, and σ is the Stefan-Boltzmann constant whose value is 5.67 x 10^{-12} W/cm^2 °C. It is expected that the conductive heat loss from the work piece's bottom surface has an exceptionally high heat transfer coefficient. On the findings of earlier research [13], this presumption is made. Using the heat flux loss by convection equation, an approximation of the heat loss was made.

$$q_b = \beta_b(T - T_0) \quad (9)$$

The boundary conditions used in the simulation presented here were adapted from Kareem N. Salloomi's work [13], and they apply a convectional coefficient of 10 W/m² °C at an ambient temperature of 25 °C to the top and side surfaces and a larger coefficient of heat transfer of 1000 W/m² °C to the bottom surface.

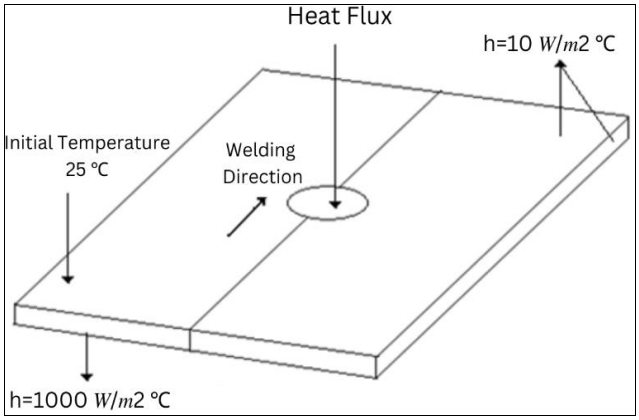

Fig 3: Schematic Representation of Boundary Conditions for Thermal Analysis

A. Heat Flux Input

A 3D heat transfer element was used for the thermal analysis, and an auto adapting heat source was employed via the user subroutine DFLUX, a FORTRAN-coded user interface provided by ABAQUS/Standard. The user subroutine instantly computed and recorded the fluctuating torque of the tool during the thermal analysis in a file. Thus, to calculate the heat generation at the tool shoulder/work piece interface, the formula [17] used is:

$$Q_{Shoulder} = \frac{4\pi^2}{3}\mu Np(r_S^3 - r_P^3) \quad (10)$$

Where, r_S and r_p stands for shoulder and pin radius, respectively. The heat produced at the contact between the tool pin and the work piece is equivalent to:

$$Q_{Pin} = \frac{4\pi^2}{3}\mu Np(r_P^3 - 3r_P^2 h) \quad (11)$$

Where, h is the pin's length. As a result, the amount of heat produced overall at the tool/work piece interfaces will be equal to:

$$Q_{Total} = \frac{4\pi^2}{3}\mu Np(r_S^3 + 3r_P^2 h) \quad (12)$$

Using the tool geometry's numerical values in the current study ($r_S = 10$ mm, $r_p = 2$ mm and $h = 4.7$ mm), the total heat generated will be calculated. It is presupposed in these equations that the tool's pressure p, is delivered uniformly.

ISSN No:-2456-2165 https://doi.org/10.38124/ijisrt/IJISRT24JUL1249

Table 3: FSW Parameters Used in the Current Study along with Heat Flux Values

Designation	Rotational Speed (rpm)	Translational Speed (mm/min)	Heat Flux Input (Q) (Watt)	Q/A (Watt/m2)
A	300	40	464.63	1.479×10^6
B	400	40	619.54	1.972×10^6
C	300	60	464.63	1.479×10^6
D	400	60	619.54	1.972×10^6

IV. MECHANICAL MODELLING

The creation of the mechanical model is the subsequent stage in the thermo-mechanical analysis. The mechanical model is fed with the temperature distributions that were discovered by the thermal study. The residual stresses caused by welding are estimated using this model. The history of measuring heat collected during the heat evaluation was entered into the programme for analysis on a foundation of the sheet being enclosed by fixings and in boundary condition form as a "predefined" field in order to identify residual stress. The programme then interpolated material properties, such as the thermal expansion coefficient, into stress elements while calculating points and in each increment of time. Because stress analysis will not cause it to alter, the heat history is considered "predefined" for this cause. To provide a coherent fluctuation of thermal and mechanical strain, the temperature interpolation is typically approximated. Given that FSW is a solid- state procedure and does not undergo phase shift, the force equilibrium equation may be written as follows using the continuum mechanics model:

$$\int_s t ds + \int_v f dV = 0 \tag{13}$$

Where, V stands for the volume that a bodily portion occupies. S is the surface enclosing this volume. At a point of S, the Cauchy stress matrix is defined as follows:

$$t = n.\sigma \tag{14}$$

Where, n is the point's unit outwards perpendicular to S. The differential equation of linear equilibrium is created by applying the Gauss theorem, which transforms a surface integration into a volume integration. Because the volume is arbitrarily determined, this equation has to be applied point-wise throughout the body:

$$\left(\frac{\partial}{\partial x}\right) \cdot \sigma + f = 0 \tag{15}$$

Substitutes these three differential equations of equilibrium in Abaqus for creating a displacement-interpolation FE model. The virtual work statement can be expressed as follows:

$$\int_S t.\delta v \, dS + \int_V f.\delta v \, dV = \int_V \sigma : \left(\frac{\partial dv}{\partial x}\right) dV \tag{16}$$

Only forces applied by thermal expansion were examined since the current study solely considers thermal residual stresses. To provide a coherent fluctuation of thermal and mechanical strain, the temperature interpolation in the stress element is typically approximated. The structural model was developed under some presumptions i.e., deformation happens symmetrically across the welded line, the substance of the plates is homogenous and there is no periodic thermal load present, hence the impact of creep is disregarded. For the modelling of the plate, DC3D8R from the heat transfer model analysis is replaced by a structural element with eight nodes (i.e., C3D8R). The structural analysis uses the same mesh design that was created for the thermal study. For the mechanical stress evaluation, the subsequent boundary conditions are employed: The work piece's vertical motion is restricted at the bottom surface. The work piece is stabilized by clamping. At these clamping points, completely rigid boundary constraints are implemented. The clamping restrictions are lifted once the weld reaches room temperature. Displacements along the symmetric surface are restricted. The choice of a complete Newton-Raphson option for solving nonlinear equations reflects the method's sophisticated approach to handling intricate interactions.

When the produced stress surpasses the material's yield point, the FSW procedure starts to exhibit plastic behavior. Stress and strain have a nonlinear relationship, which defines plasticity. In the present thermomechanical analysis, Johnson–Cook's (JC) plasticity model is employed. The Johnson-Cook model (JC), which describes how the flow stress is connected to strain, strain rate, and temperature, was used to characterize the structural model of AA 2024-T3 and AA 5086-O alloys during FSW process:

$$\sigma = (A + B\varepsilon^n)\left[1 + C\ln\left(1 + \frac{\dot{\varepsilon}}{\dot{\varepsilon}_0}\right)\right]\left[1 - \left(\frac{T - T_{room}}{T_{melt} - T_{room}}\right)^m\right] \tag{17}$$

The Johnson-Cook model combines the thermal reaction (temperature increase) with the mechanical response (plasticity). Here mechanical deformation and temperature distribution are closely correlated, this linkage is crucial for analysis.

ISSN No:-2456-2165 https://doi.org/10.38124/ijisrt/IJISRT24JUL1249

Table 4: JC Model Constants for Aa 2024-T3 & Aa 5086-O [13] [18]

Material	A (MPa)	B (MPa)	n	C	m	T_{melt} (℃)	T_{room} (℃)
AA2024-T3	369	684	0.73	0.0083	1.7	521	25
AA5086-O	170	425	0.42	0.0335	1.225	640	25

V. RESULTS AND DISCUSSION

The discussion in the present part centers on the numerical results of the thermal and residual stress conditions created by FSW's joining of AA 2024-T3 and AA 5086-O. As we already said, the AA 2024-T3 alloy was placed on the advancing side, while the AA 5086-O alloy was on the retreating side. In FSW of the same dissimilar alloys, two translational rates of 40 and 60 mm/min were combined with two rotating speeds of 300 and 400 rpm.

A. Influence of process parameters on thermal cycles

The main topic of discussion in this section is how two important weld factors, "Translational Speed" and "Rotational Speed", affect the thermal cycles that the welding plates go through throughout the welding process. These two variables play a key role in deciding how quickly the welding process moves along. The examination of simulated temperature data is used to determine the relevance of these two parameters, which is the main objective. The thermal cycles of the weld plates refers to the temperature swings that the plates experience while being welded. Due to the friction and deformation involved in welding, a lot of heat is produced. The distribution of residual stresses and microstructure of the material are all impacted by this heat. As shown in figure 1, temperature profiles were taken at 15 mm away from weld centerline on both AA 2024-T3 (advancing side) and AA 5086-O (retreating side).

Figure 4 shows how utilizing various stirring tool rotational speeds (300 & 400 rpm) affects the temperature profile. The below graphs emphasizes the fact that the amount of heat produced will grow proportionally as the tool's rotational speed is raised. Figure 4 displays the temperature variation all through the plate perpendicular to the weld direction. It has been found that increasing tool rotating speed raises the temperature distribution of the weld sample on both the advancing and retreating sides as a result of higher heat input. While welding dissimilar aluminum alloys (AA2024-T3 and AA6061-T6) by FSW, Kareem N Salloomi [13] obtained similar results. Similarly, H. Jamshidi Aval [9] obtained the similar results while doing the FSW of dissimilar aluminum alloys of AA5086-AA6061. Additionally, it is noted from the temperature profiles that the peak temperature in the welded region is more affected by tool rotational speed.

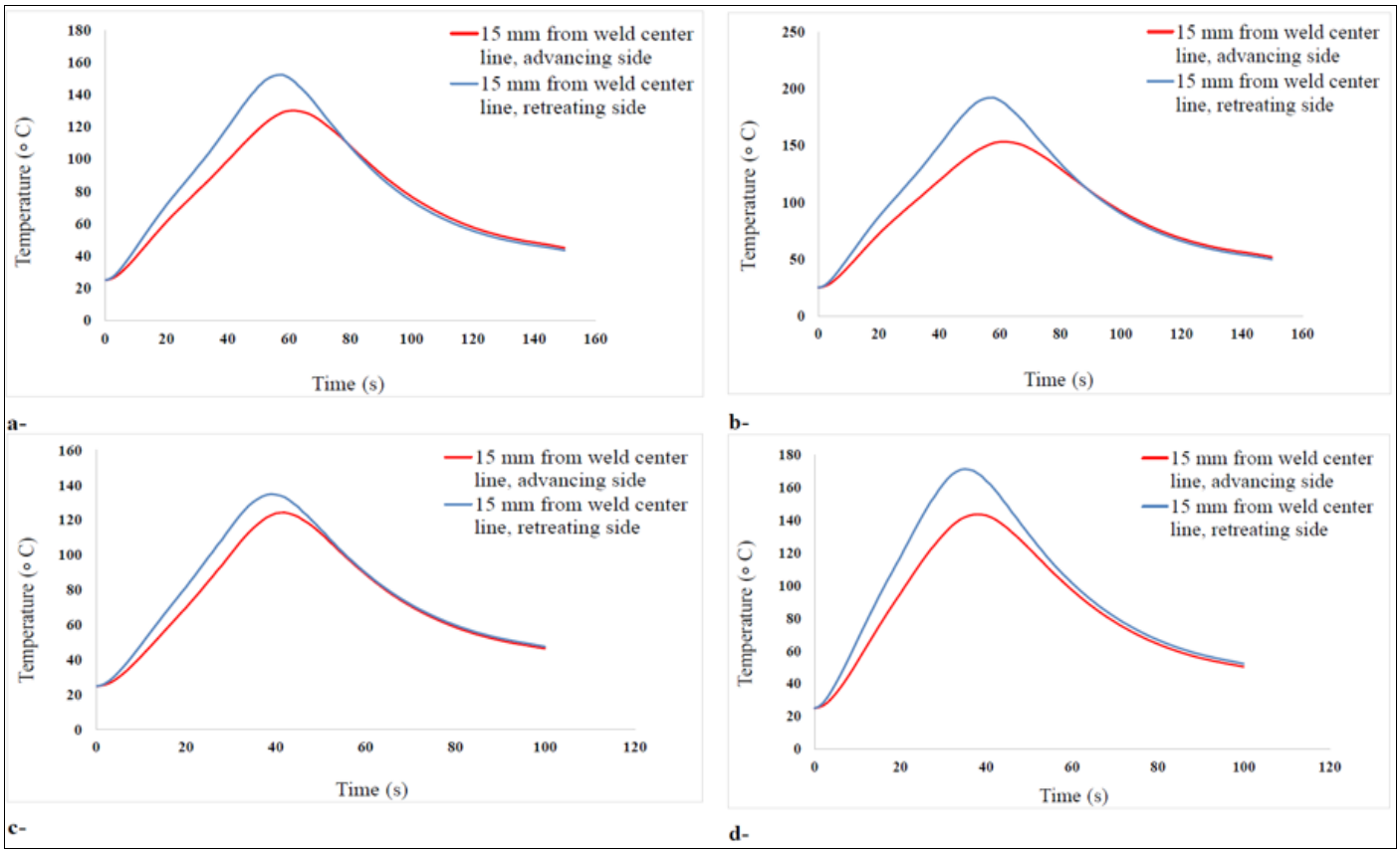

Fig 4: Effect of FSW Working Parameters on Temperature Distribution at 15 mm from Weld Center Line: a-Case A, b- Case B, c- Case C, d-Case D

ISSN No:-2456-2165 https://doi.org/10.38124/ijisrt/IJISRT24JUL1249

In this numerical study, for the situation of a traverse speed of 40 mm/min, the 400 rpm rotational speed produced a larger peak temperature than the 300 rpm, as shown in Fig. 4 (a, b). The case of 60 mm/min, as indicated in Fig. 4 (c, d), is the same. Increased rotational speed causes the tool and substance to come into fast and intense contact through friction. Greater heat is generated at the contact as a consequence. The material has less time to dissipate the heat produced due to the faster spinning speed. Higher rotational speed causes the tool to travel around the joint more quickly, giving heat in the surrounding material less time to disperse. Because of this, the weld zone retains more heat. Higher rotational speed improves the tool's ability to mix and stir. This improves heat dispersion throughout the material, raising the temperature of the metal being joined even more. To obtain the appropriate welding results for diverse aluminum alloys, a balance must be established between rotating speed, heat production, and overall process stability. Furthermore, it is noticed from the four cases of Fig. 4, the temperature distribution on the retreating side (AA5086-O) is somewhat greater as compared to the value of the temperature on the advancing side (AA2024-T3).

Similarly, the temperature profile is affected by using different tool translational speeds (40 and 60 mm/min), as seen in Fig. 4. From the figure, it can be observed that the highest temperature was reduced in both the advancing and retreating sides when the traverse speed was raised from 40 mm/min to 60 mm/min. The findings reached by Pankaj et al. [19] are in excellent accord with the results established above. In this numerical study, for the case of a rotational speed of 300 rpm, the 40 mm/min translational speed produced a larger peak temperature than the 60 mm/min, as shown in Fig. 4 (a, c). The case of 400 rpm, as indicated in Fig. 4 (b, d), is the same. The tool passes the weld joint more quickly as its translational speed rises. This indicates that there is less time for the spinning tool and the substance to interact. Lower temperatures are the result of shorter contact times since less time is allowed for heat to accumulate. This is due to the tool moving more quickly, which results in less heat being produced per unit length of the weld. Lower temperatures come from less extreme plastic deformation of the material due to faster tool speeds. The quantity of heat delivered to the material is constrained by the shorter contact duration. Although greater tool speeds often result in lower temperatures, it's crucial to keep in mind that there must be a careful balance struck since very high speeds may negatively impact the quality of the weld joint owing to insufficient heat generation for effective plastic deformation and material mixing.

According to the four cases in Figure 4, the temperature distribution on the retreating side is somewhat greater than the value on the advancing side. The variation is made because AA 2024 alloy's latent heat on the advancing side absorbs heat, while AA 5086 alloy's latent heat loss rate on the retreating side is less than AA 2024 alloy.

B. Temperature Profile at the End of Welding Stroke

The temperature profile in FSW of dissimilar aluminum alloys displays fascinating behavior towards the finishing of the welding stroke. The temperature inside the stirring zone of various workpieces remains consistently stable as the tool advances along the welding path.

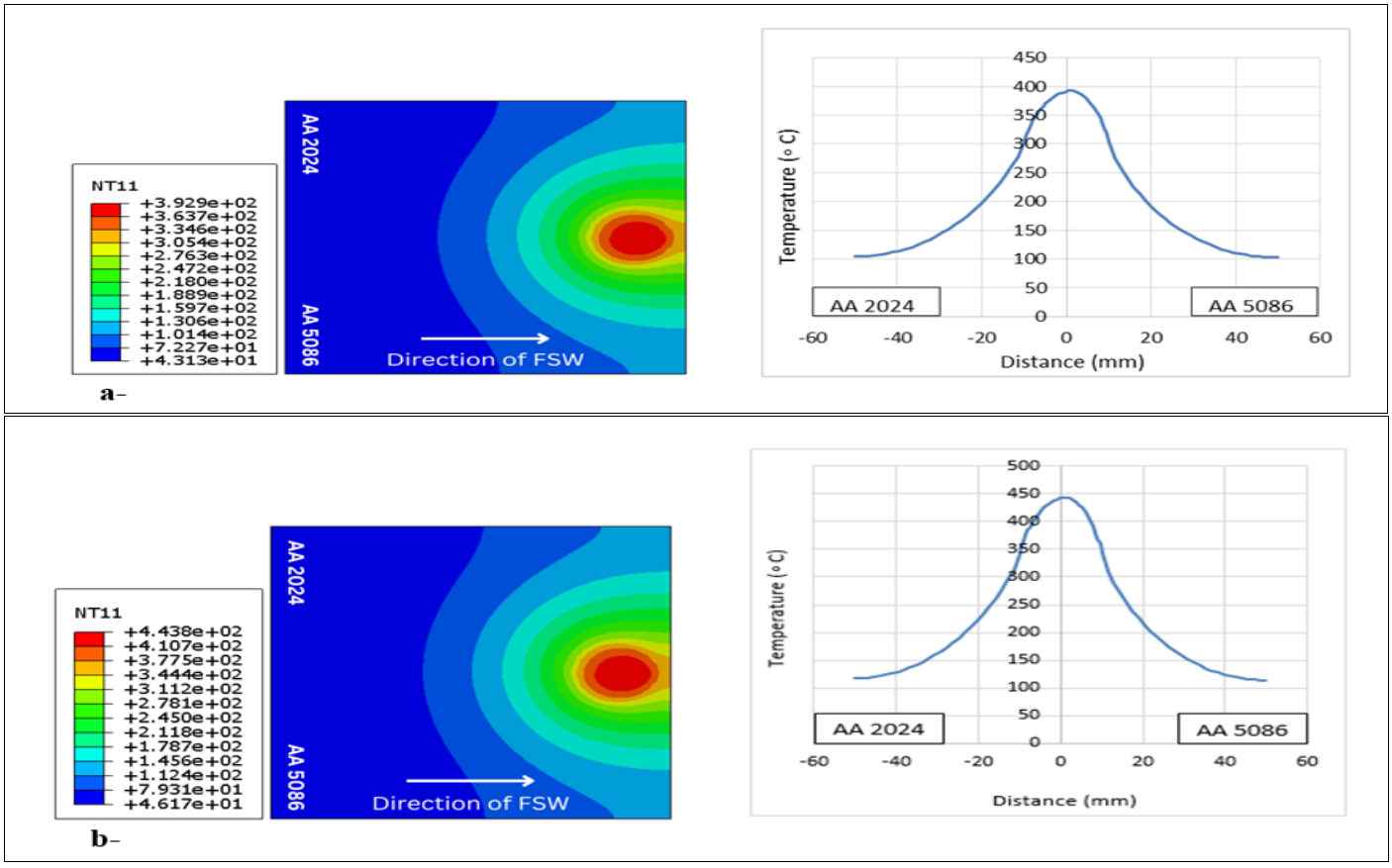

ISSN No:-2456-2165 https://doi.org/10.38124/ijisrt/IJISRT24JUL1249

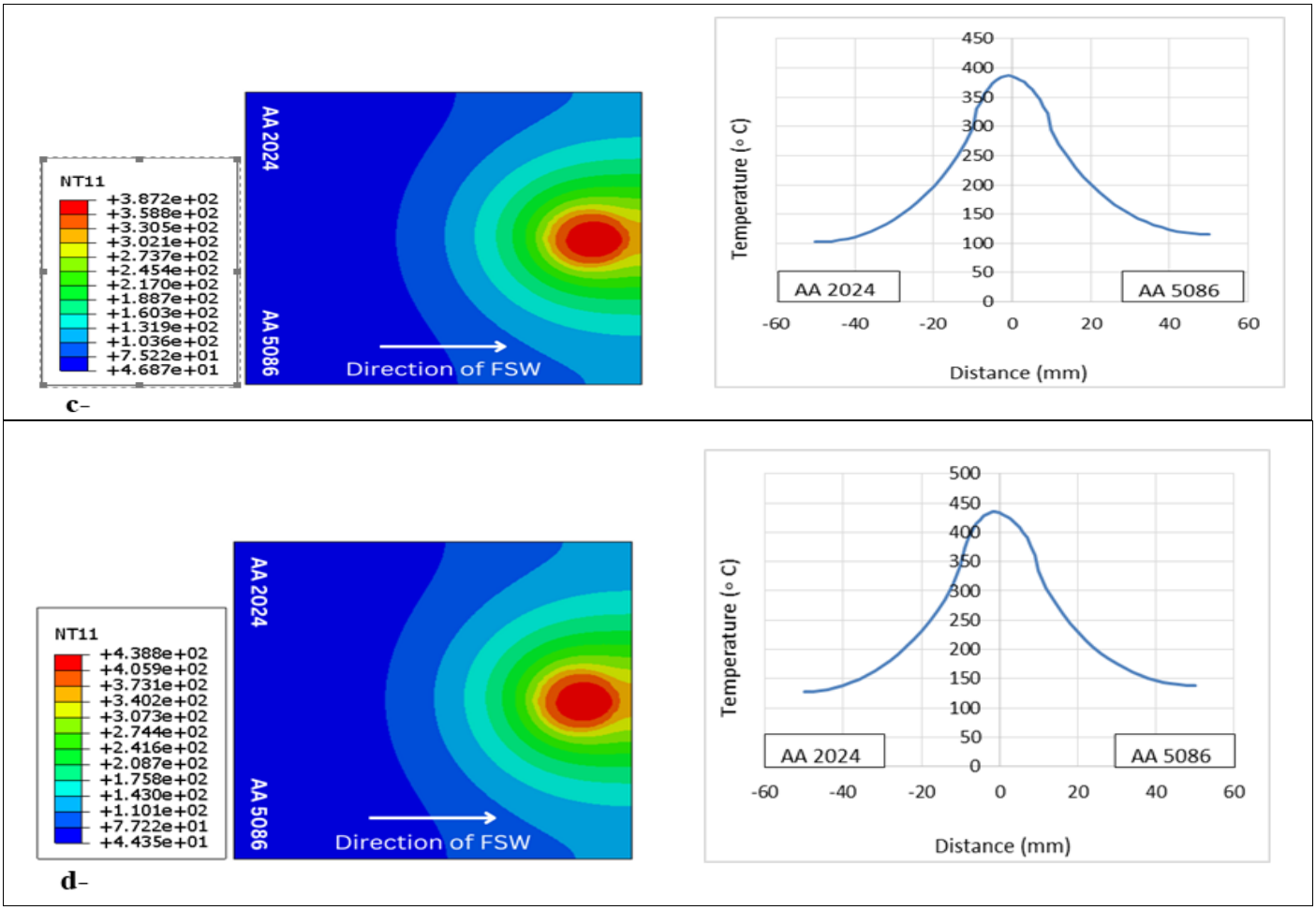

Fig 5: Temperature Distribution Across the Width of the Dissimilar FSW Sample at the End of Welding Stroke: a- Case A, b- Case B, c- Case C, d- Case D

This temperature remains virtually unchanged before the tool nears the completion of the welding cycle. This sustained temperature is primarily attributed to the continuous generation of frictional heat resulting from the tool's rotational engagement with the metal. To elaborate, as the welding tool travels through the workpiece, it encounters resistance and friction at the contact between the tool and the metal. This friction generates heat, which is continuously produced throughout the welding method. As a result, the temperature within the region where the metal is being stirred and fused remains relatively constant. The graphs demonstrate how the temperature first adopts an asymmetrical temperature value outside of the stirring zone, but maintains a rather symmetrical distribution inside. As previously noted, this might be attributed to the two incompatible alloys' different thermal material qualities as well as the uneven heat production rates at each component. Furthermore, it was discovered that in all the four cases, the temperatures observed during the FSW process were lower as compared to the corresponding melting points of AA2024-T3 and AA5086-O. This is significant because it demonstrates that there was no phase transition from the solid to liquid state of the components. Instead, the entire process took place in the solid form and this demonstrates the solid-state joining nature of FSW. This finding emphasizes how solid-state FSW is as a non-fusion joining method.

C. Influence of Process Parameters on Residual Stresses

The internal stresses that are still present in a welded joint after the welding process is over and the material has cooled down are termed as residual stresses in FSW. The complicated temperature cycles, plastic deformation, and phase changes that occur throughout the FSW process are a few of the causes of these stresses. The mechanical characteristics of the welded junction and the surrounding material might be impacted by residual stresses. They may affect things like overall structural integrity, fracture toughness, and fatigue life. High residual stress levels might cause the welded component to break early or function less well. In the welded structure, residual stresses may result in distortion, warping, and dimensional changes. This is especially difficult for precision applications like aerospace or automotive parts, where precise dimensions and alignments are essential. Particularly in settings where corrosive chemicals are prevalent, elevated residual stresses can produce areas of high stress concentration, making the welded joint more liable to cracking and stress corrosion cracking. Therefore, accurately predicting, controlling, and mitigating residual stresses are crucial for ensuring the reliability and durability of welded components.

ISSN No:-2456-2165 https://doi.org/10.38124/ijisrt/IJISRT24JUL1249

The temperature history of the FSW of dissimilar aluminum alloys has a significant impact on the formation of residual stresses within the welded specimen. The amount of thermal expansion and contraction of the materials depends on how quickly the materials are heated and cooled during FSW. Thermal gradients within the welded joint can be caused by rapid heating and cooling. As the material tries to adapt to these temperature-induced changes, these gradients cause non-uniform expansion and contraction, which causes the creation of residual stresses. FSW is a solid-state welding method, which means that no melting occurs when welding. Instead, in high temperatures, they experience extreme plastic deformation. FSW can undergo substantial plastic flow and recrystallization. Due to the tool's rotation and translation, which result in varied strain and strain rate across several weld locations, the deformation patterns are complicated. Localized plastic strain is produced as a result, and residual stresses are later developed. Using a sequential simulation, the numerical analysis of residual stresses was carried out. The mechanical model is fed with the temperature distributions that were discovered by the thermal study. The residual stresses produced by welding are estimated using this model. The history of measuring heat collected during the heat analysis was entered into the programme for analysis on a foundation of the sheet being enclosed by fixings and in boundary condition form as a "predefined" field in order to identify longitudinal residual stresses. The programme then interpolated material properties, such as the thermal expansion coefficient, into stress elements while calculating points and in each increment of time. It is crucial to remember that the residual stress computation was performed after the cooling period's last stage was completed (i.e., after 100 seconds of welding).

In FSW, the predominant longitudinal stress component is a consequence of the interaction between plastic deformation and anisotropic behavior. So, compared to the transverse component, the longitudinal stress factor is the dominating stress [13]. The existence of a welding fixture provides significant mechanical limitations that have a significant impact on how residual stresses are distributed. It's interesting to note that the maximum residual stress magnitude has been seen to decrease when these fixtures are removed quickly after the welding operation. In this section, we can see from the figure 6 and figure 7 that how the tool rotational speed and translational speed in FSW of dissimilar aluminum alloys significantly influence the growth of longitudinal residual stresses within the connected joint. Figure 6 shows the contours of longitudinal residual stresses without clamping and figure 7 shows the spatial distribution of longitudinal residual stresses with and without clamping. The red line's path indicates the distance at which the graphical distribution was plotted as shown in figure 6.

The graphs in figure 7 show that a reduction in longitudinal residual stress levels occurs when the tool's rotational speed is raised from 300 rpm to 400 rpm. This finding is in line with the results reached by Zapata and colleagues in their 2016 investigation [11] when they increased the rotating speed from 550 rpm to 840 rpm, they saw a similar result. Higher rotational speeds have an impact on heat production and temperature distribution over the surfaces of the dissimilar joint, which explains why this phenomena occurs. Increased frictional heat production between the tool and workpiece is a result of faster rotating speeds. This increased heat drains into the surrounding material more efficiently, minimizing localized overheating. The outcome is a decrease in the steepness of the temperature gradients inside the welded zone, which reduces the development of large thermal gradients that may result in residual stresses.

ISSN No:-2456-2165 https://doi.org/10.38124/ijisrt/IJISRT24JUL1249

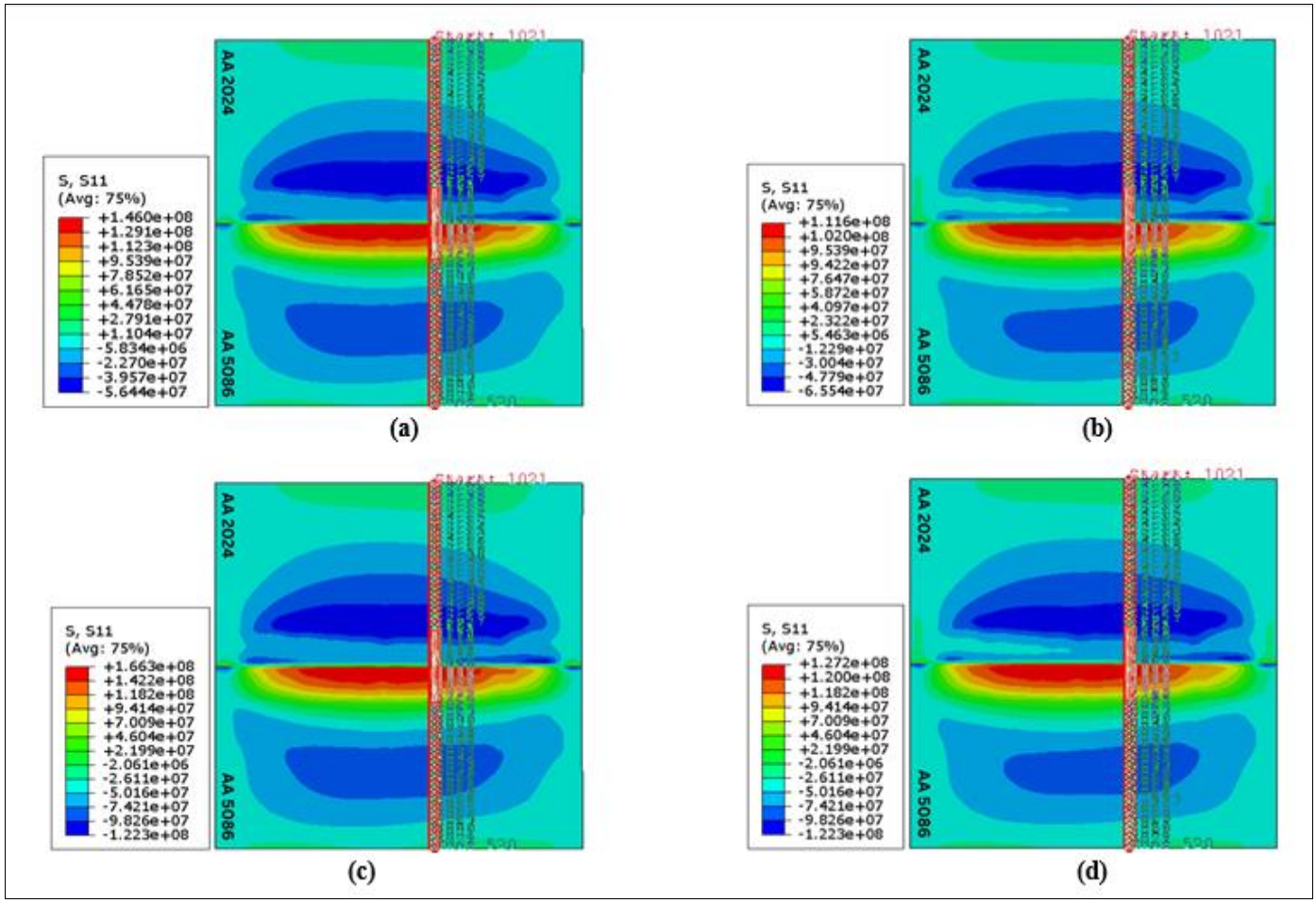

Fig 6: Longitudinal Residual Stresses Contours without Clamping: a- Case A, b- Case B, c- Case C, d- Case D

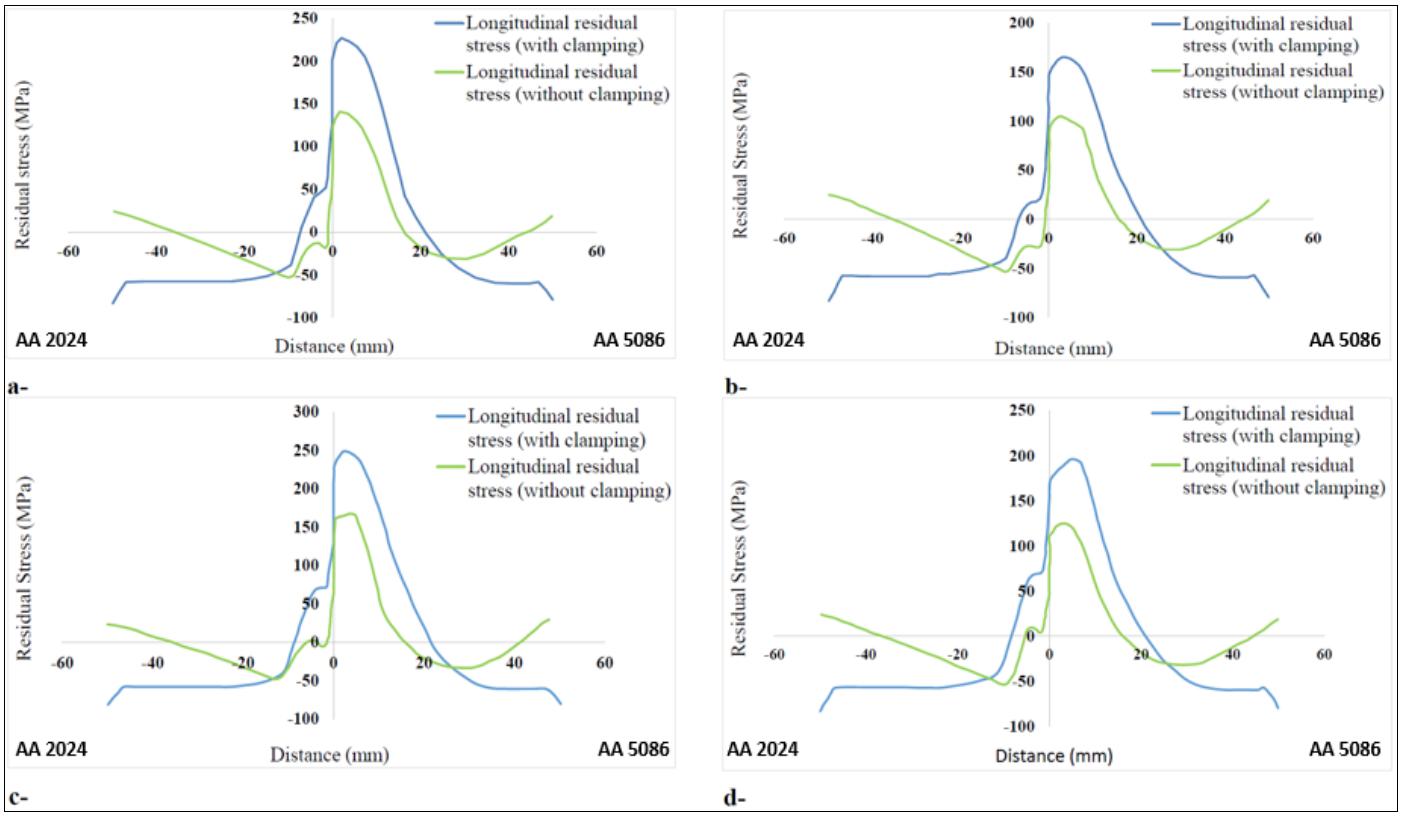

Fig 7: Spatial Distribution of Longitudinal Residual Stresses with and Without Clamping Along the Red Path: a- Case A, b- Case B, c- Case C, d- Case D.

ISSN No:-2456-2165 https://doi.org/10.38124/ijisrt/IJISRT24JUL1249

For case A (without clamping), the greatest longitudinal residual stresses in finite elements was 140.4 MPa, whereas for case B (without clamping), the greatest longitudinal residual stresses was 105.12 MPa. So there is a significant decrease in the value of longitudinal residual stresses when rotational speed is raised from 300 to 400 rpm with constant translational speed of 40 mm/min. Similar trend was noticed when the rotational speed is raised from 300 to 400 rpm in cases C and D when the traverse speed is constant at 60 mm/min. For case C, the greatest longitudinal residual stresses in finite elements was 166.96 MPa and for case D, it was 124.64 MPa. Overall, the altered thermal and mechanical behavior of the welded materials as a result of the increased tool rotating speed leading to a more even and balanced distribution of stress.

The data from figures 6 and 7 demonstrates that, for both 300 rpm and 400 rpm, raising the translational speed from 40 mm/min to 60 mm/min causes a rise in longitudinal residual stresses in the welding's core area. This is reliable with the conclusions of Zapata et al. [11], who found that when traverse speed rose, longitudinal residual stresses also increased. Faster translational rates might cause the material to heat and cool inequitably. A faster translational speed might make the material mix over the weld zone less efficient. The mixing motion used in friction stir welding helps to distribute and ease the tension. Rapid tool movement can restrict mixing and increase the possibility of residual stress buildup by causing localized stress concentrations. For case A (without clamping), the greatest longitudinal residual stresses in finite elements was 140.4 MPa, whereas for case C (without clamping), the greatest longitudinal residual stresses was 166.96 MPa. So there is a significant increase in the value of longitudinal residual stresses when translational speed is raised from 40 to 60 mm/min with constant rotational speed of 300 rpm. Similar trend was noticed when the translational speed is increased from 40 to 60 mm/min in cases B and D when the rotational speed is constant at 400 rpm. For case B, the greatest longitudinal residual stresses in finite elements was 105.12 MPa and for case D, it was 124.64 MPa.

The findings also indicate that the retreating side has larger residual stresses than the advancing side in all the four cases. This phenomena can be explained by elements like the stronger temperature environment and more plastic strain encountered by the retreating side in comparison to the advancing side.

D. Effect of Clamping on Residual Stresses

It has been observed that the distribution of residual stresses in a welded joint is significantly influenced by the mechanical restriction imposed by the welding fixture/clamping. When a welding fixture is used during the friction stir welding procedure, it limits how much the workpiece may move and change shape as it warms and cools. This restriction may cause larger residual stresses to develop in some parts of the welded joint. But when the fixtures are taken out right away after the welding, the welded joint is given more range of motion and relaxation [20]. As a result, any accumulated residual stresses that were brought on by the fixture's restrictions can now be distributed and released more easily.

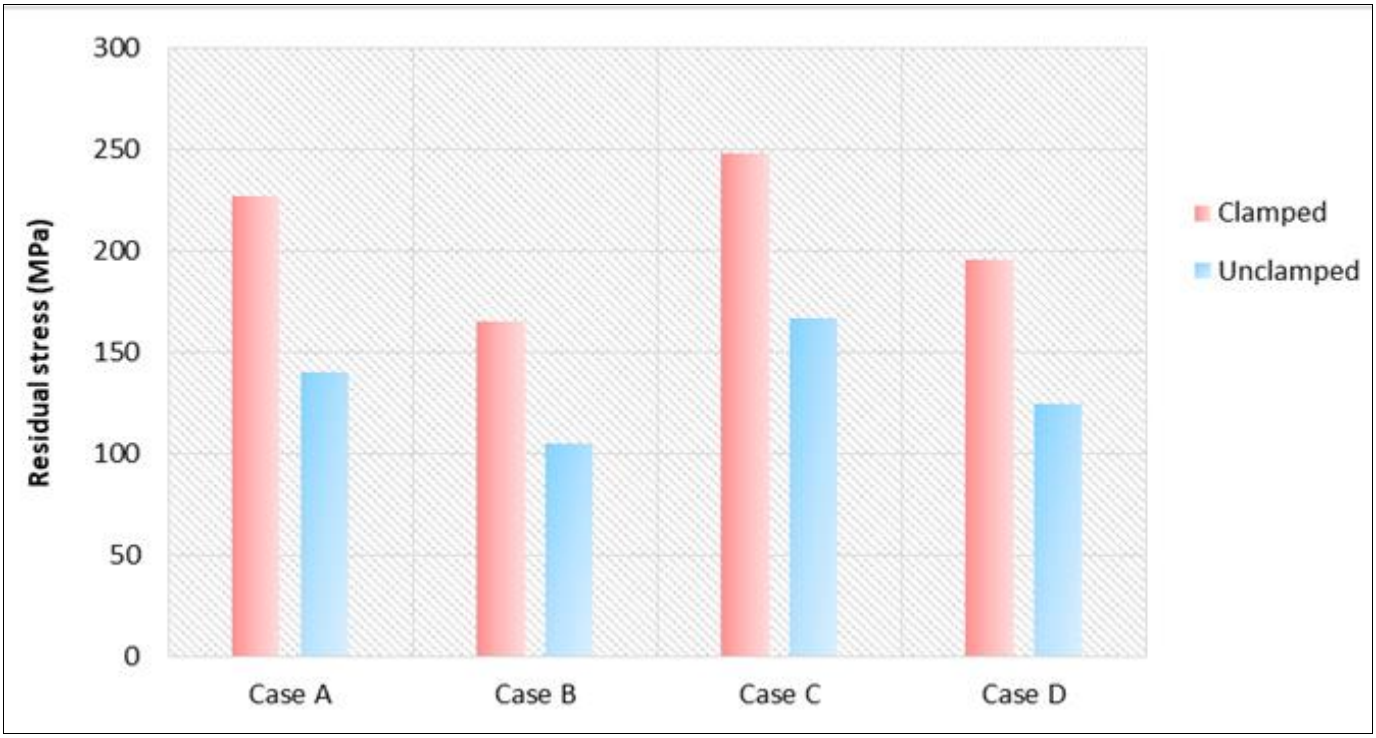

Fig 8: Comparison of Residual Stresses Between Clamped and Unclamped Workpiece

ISSN No:-2456-2165 https://doi.org/10.38124/ijisrt/IJISRT24JUL1249

Therefore, the use of welding fixtures results in a restricted environment that influences the formation of certain residual stress patterns throughout the welding method. The maximum residual stress levels within the welded joint are decreased when the fixtures are removed after welding because this allows the stresses to be redistributed and relaxed, as shown in figure 8. In order to guarantee the appropriate mechanical qualities and structural integrity of the welded components, it is crucial to take this phenomena into account.

VI. VALIDATION OF FEM MODEL

It is crucial to compare the produced model with the results that has been published in order to validate the thermomechanical model that had been created using ABAQUS. Kareem N Salloomi's numerical findings [13] were used to validate the created thermomechanical model for this purpose. The numerical modeling for friction stir welding (FSW) involved two dissimilar aluminum plates, namely AA 2024-T3 and AA 6061-T6 alloys. Case C of the above mentioned research was used for the validation of thermal and residual stress values.

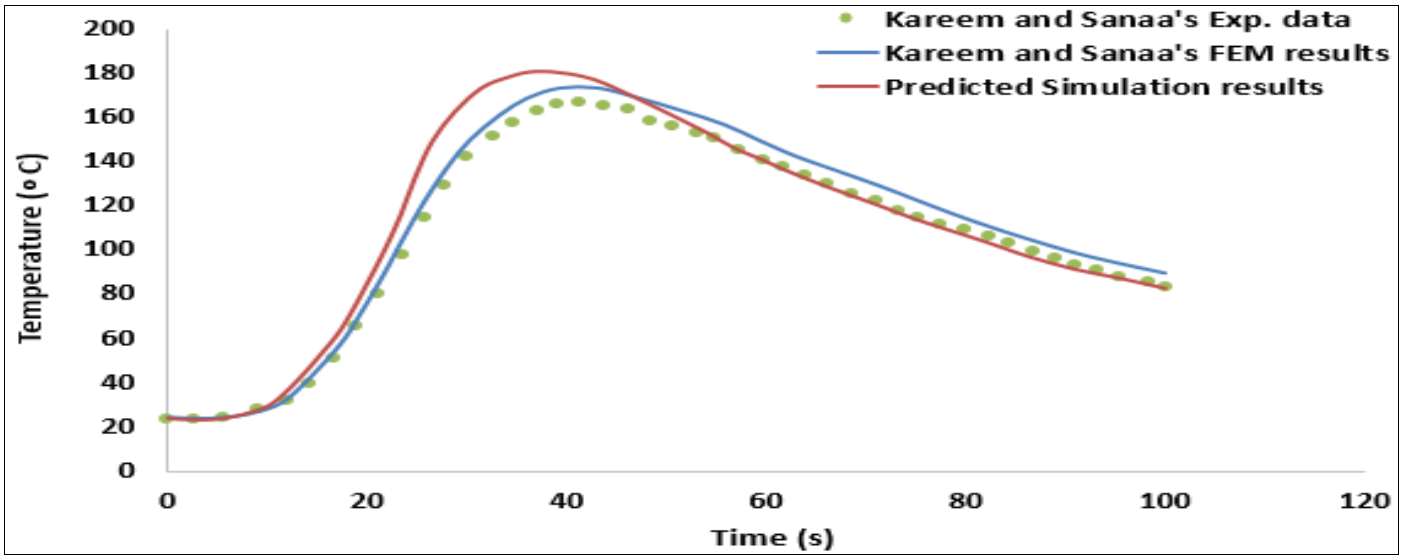

Fig 9: Comparison of Temperature Distribution Along Advancing Side at 15mm away from Joint Line

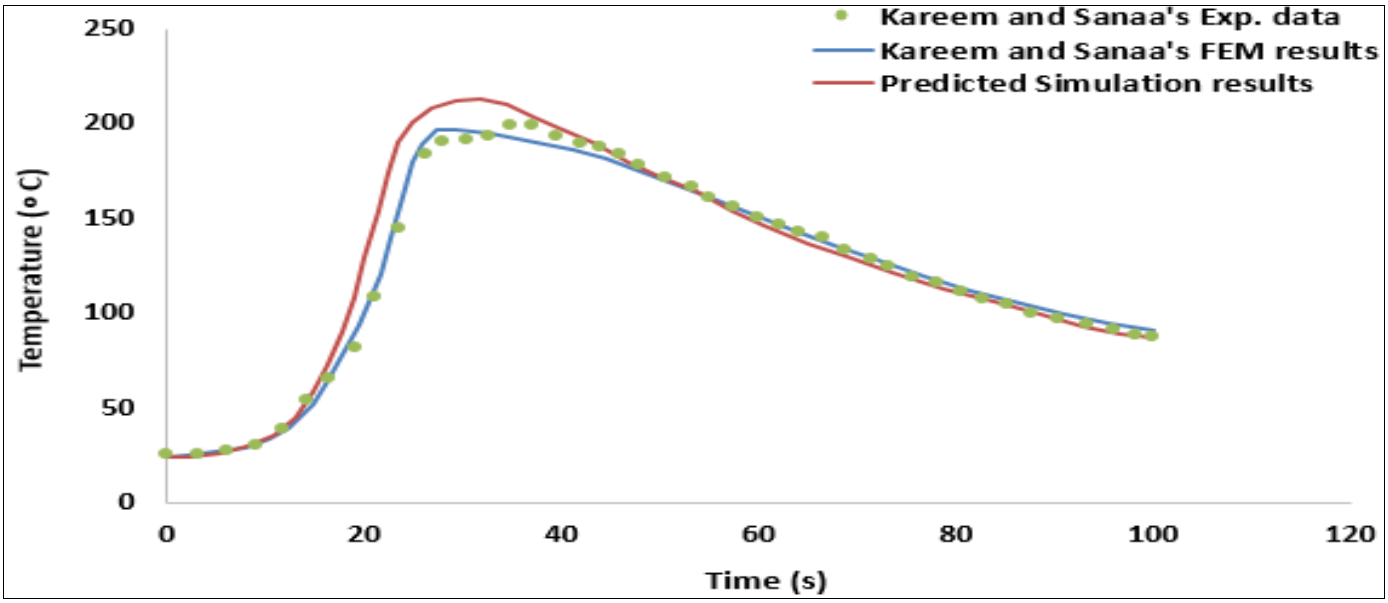

Fig 10: Comparison of Temperature Distribution Along Retreating Side at 15 mm Away from Joint Line

Both the thermal profiles (at advancing and retreating sides) were deduced at the same point at which authors (Kareem and Sanaa) deduced the thermal histories. The results show that at advancing side, the maximum temperature from predicted simulation results is 180.45 whereas the maximum temperature observed by the author was 173.11. Therefore, it means that the predicted value overvalued the author's value by 4.24%. Whereas, at retreating side, the maximum temperature from predicted simulation results is 210.34 whereas the maximum temperature observed by the author was 197.45. Therefore, it means that the predicted value overrated the author's

ISSN No:-2456-2165 https://doi.org/10.38124/ijisrt/IJISRT24JUL1249

value by 6.53%. As a result, the validity of the model created in this work is confirmed. The general trend of the anticipated temperature profile is comparable to that found by Kareem and Sanaa [13]. Similarly, the predicted residual stress values were compared with already published results.

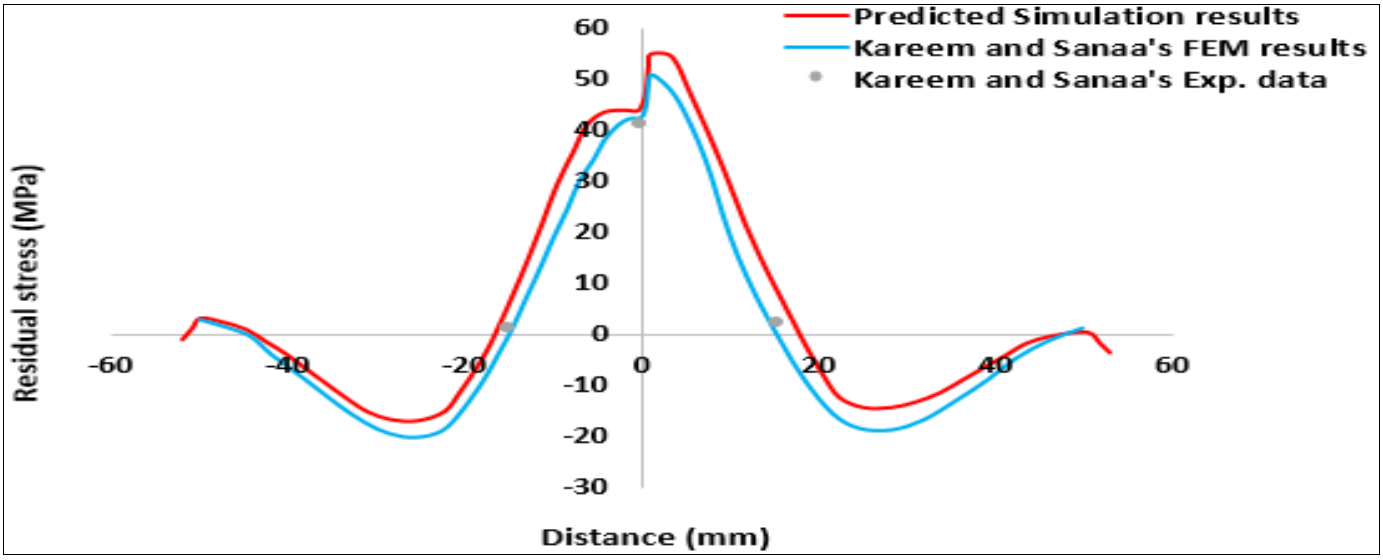

Fig 11: Variation of the Longitudinal Residual Stress Along the Specified Path

Figure 11 compares the simulation results for longitudinal residual stresses along the specified path with the findings from Kareem and Sanaa. The receding side was found to have considerably higher residual stresses. The output specify that the maximum longitudinal residual stress from predicted simulation result is 54.72 MPa whereas the max longitudinal residual stress observed by the author was 50.89 MPa. Therefore, it means that the predicted value overestimated the author's value by a percentage of 7.53%. The general trend of the created model for residual stress prediction is in good co-relation with that of Kareem and Sanaa [13], demonstrating the model's validity.

VII. CONCLUSIONS

The goal of the study was to determine how different tool rotational and traverse rates affected the final thermal and residual stress distributions. AA 2024-T3 was positioned in this inquiry on the advancing side and AA 5086-O was on the retreating side. The study discusses the subsequent conclusions:

- The sequentially coupled thermal-stress finite element technique has a clear benefit for determining temperature profiles and resultant residual stress distributions in dissimilar FSW of aluminium alloys.
- The thermal model can ascertain temperatures across various friction stir weld zones, demonstrating that both tool rotation and translation speeds influence peak temperatures. Notably, tool rotation speed exerts a more substantial effect on weld zone temperature compared to translation speed.
- Across all four examined cases in the present study, the temperature consistently remained higher on the AA 5086 side. As the tool's rotational speed increased, the temperature distribution grew proportionally, with AA 5086 maintaining its temperature superiority. Conversely, a higher welding traverse speed caused a relatively modest reduction in temperature distribution.
- Thermomechanical model was used to simulate the residual stress fields in the welded plates in order to better understand how they were distributed. The longitudinal residual stress component was determined, it was discovered that the AA 5086 side had a greater value of residual stresses than the AA 2024 side. As the tool rotational speed rose, the magnitude of this residual stress component dropped, however it showed an increase with greater tool translational speeds.
- The obtained results for residual stresses affirm that the tool's rotational speed exerts a more significant influence compared to the tool's traverse speed.
- Observations indicate that the presence of a welding fixture exerts significant influence over the distribution of residual stress, and the timely removal of these fixtures notably diminishes maximum residual stress levels.

REFERENCES

[1]. W. M. Thomas, M. G. Murch, E. D. Nicholas, P. T. Smith, J. C. Needham and C. J. Dawes.Welding Institute England Patent EP0653265A2, 1991.

[2]. S. A. A. A. Mousavi and S. H. S. , "Dissimilar Friction Stir Welds in AA 5086–AA 2024: The Effect of Process Parameters on Microstructures and Mechanical Properties," *Advanced Materials Research*, vol. 445, pp. 753-758, 2012.

[3]. G. J. E and F. Z., "Preliminary modeling of the friction stir welding process," in *EWI*, Columbus,Ohio,US, 1996.

ISSN No:-2456-2165 https://doi.org/10.38124/ijisrt/IJISRT24JUL1249

[4]. A. I. P. Almanar, M. S. B. Shaari and M. S. Jaffarullah, "Temperature Distribution in Friction Stir Welding Using Finite Element Method," *International Journal of Mechanical and Mechatronics Engineering*, vol. 8, no. 10, 2014.

[5]. A. Arif, C. Swaroop and K. N Pandey, "TEMPERATURE VALIDATION FOR FRICTION STIR WELDING (FSW) OF DISSIMILAR ALUMINUM ALLOYS," in *International Conference on Advances in Mechanical Engineering, ICAME-2013*, Pune, Maharashtra, 2013.

[6]. M. J. Peel, A. Steuwer and M. Preuss, "Microstructure, mechanical properties and residual stresses as a function of welding speed in aluminium AA5083 friction stir welds," *Acta Materialia*, vol. 51, p. 4791–4801, 2003.

[7]. C. Chen and R. Kovacevic, "Finite element modeling of friction stir welding—thermal and thermomechanical analysis," *International Journal of Machine Tools and Manufacture*, vol. 43, no. 13, pp. 1319-1326, 2003.

[8]. H. Zhang, Z. Zhang and . J. Chen, "The finite element simulation of the friction stir welding process," *Materials Science and Engineering: A*, vol. 403, no. 1-2, pp. 340-348, 2005.

[9]. H. J. Aval, S. Serajzadeh and . A. H. Kokabi , "Experimental and theoretical evaluations of thermal histories and residual stresses in dissimilar friction stir welding of AA5086-AA6061," *The International Journal of Advanced Manufacturing Technology*, vol. 61, p. 149–160, 2012.

[10]. A. Arif and K. N. Pandey, "Thermo-mechanical Modeling for Residual Stresses of Friction Stir Welding of Dissimilar Alloys," *International Journal of Engineering Science and Technology*, vol. 5, no. 6, pp. 1195-1204, 2013.

[11]. J. Zapata, M. T. Gonzalez and D. d. J. Pérez López, "Residual stresses in friction stir dissimilar welding of Aluminum alloys," *Journal of Materials Processing Technology*, vol. 229, pp. 121-127, 2016.

[12]. N. Zina and A. Brahami, "Numerical Simulation on the Effect of Friction Stir Welding Parameters on the Peak Temperature, Von Mises Stress, and Residual Stresses of 6061-T6 Aluminum Alloy," *Journal of Failure Analysis and Prevention*, vol. 19, p. 1698–1719, 2019.

[13]. K. N. Salloomi and . S. Al-Sumaidae, "Coupled Eulerian–Lagrangian prediction of thermal and residual stress environments in dissimilar friction stir welding of aluminum alloys," *Journal of Advanced Joining Processes*, vol. 3, 2021.

[14]. I. Zuiko and S. S. Malopheyev, "Dissimilar Friction Stir Welding of AA2519 and AA5182," *Materials*, vol. 15, 2022.

[15]. K. H. Huebner, D. L. Dewhirst, D. E. Smith and T. G. Byrom, The Finite Element Method for Engineers.4th ed., New York: John Wiley & Sons, 2001.

[16]. D. Radaj, Heat Effects of Welding—Temperature Field, Residual Stress, Distortion, Berlin: Springer, 1992.

[17]. M. Riahi and H. Nazari, "Analysis of transient temperature and residual thermal stresses in friction stir welding of aluminum alloy 6061-T6 via numerical simulation," *The International Journal of Advanced Manufacturing Technology*, vol. 55, no. 1, pp. 143-152, 2010.

[18]. A. Ghiasvand, "Effects of tool offset, pin offset, and alloys position on maximum temperature in dissimilar FSW of AA6061 and AA5086," *International Journal of Mechanical and Materials Engineering*, vol. 15, no. 1, 2020.

[19]. P. Pankaj, A. Tiwari and P. Biswas, "A three-dimensional heat transfer modelling and experimental study on friction stir welding of dissimilar steels," *Journal of the Brazilian Society of Mechanical Sciences and Engineering*, vol. 42, 2020.

[20]. V. R. Trummer and E. Suzano, "Influence of the FSW clamping force on the final distortion and residual stress field," *Materials Science and Engineering: A*, vol. 538, pp. 81-88, 2012.